Supporting Information for:

Synergy of Electrolyte Manipulation and Separator Functionalization Enables Ultralong-life Nonaqueous Magnesium-Organic Batteries

Xiaolan Xue,* Tianlong Huang, Yang Zhang, Quanjie Zhong, Mengke Tang, Han Shang, Yuanxiang Zhang, Maosheng Cui, Jiqiu Qi, Huan Xu,* Yanwei Sui*

School of Materials Science and Physics, China University of Mining and Technology, Xuzhou 221116, China

*Address correspondence to xuexiaolan@cumt.edu.cn; hihuan@cumt.edu.cn; suiyanwei@cumt.edu.cn

Experimental section

Preparation of Graphene@PVP dispersion: 3 g of commercial graphite and 0.5 g of polyvinyl pyrrolidone (PVP, K30) were first added into 500 ml of deionized water. Then, the obtained mixtures were transferred into a nanobead mill and grounded for 72 hours to obtain a uniformly dispersed Graphene@PVP dispersion.

Fabrication of Graphene@PVP/GF separator: A certain volume of the as-obtained Graphene@PVP dispersion above was vacuum filtered through the commercial glass fiber separator (Whatman Grade GF/D) with a diameter of 100 mm, followed by drying at 50 °C for 24 h. The resulting Graphene@PVP-coated GF (Graphene@PVP/GF) separator was pouched into discs with a diameter of 19 mm. The weight loading of the Graphene@PVP interlayer was about 0.2 mg cm^{-2}.

Preparation of electrolyte: The preparation of $Mg(HMDS)_2$-$MgCl_2$/THF and $Mg(HMDS)_2$-$MgCl_2$/THF-PP14TFSI electrolytes were carried out in an Ar-filled glovebox with both H_2O and O_2 content below 0.01 ppm, according to the previous reports[12,S1].

Characterization: Scanning electron microscope (SEM, Zeiss Gemini 500, Germany) was utilized to determine the morphological features of the different samples. The reflectance Fourier transform infrared (FTIR) spectra were collected on a Spectrum 3 spectrometer. The crystal structure was investigated on Bruker D8 Focus powder X-ray diffractometer

(XRD) with Cu Kα as radiation source. X-ray photoelectron spectroscopy (XPS) measurements were performed by a Thermo Fisher Scientific ESCALAB 250Xi instrument using Al Kα as radiation source.

Electrochemical Measurements: The phenazine (PZ) cathode was prepared as follows: the directly purchased PZ powder, acetylene black, and poly(vinylidene fluoride) (PVDF) were mixed at a mass ratio of 6:3:1 and then ground in a mortar for half an hour. An appropriate amount of 1-methyl-2-pyrrolidinone (NMP, >99%) was then added into the above powder mixture and stirred continuously for 6 h. The resulting homogeneous slurry was scraped onto the carbon paper and dried in a vacuum oven at 50 °C for 24 h. Coin 2032 cells were assembled with PZ cathode, modified Graphene@PVP/GF separator or pristine GF separator, $Mg(HMDS)_2$-$MgCl_2$-based electrolyte, and Mg foil anode in an Ar-filled glovebox. The loading mass of active materials in the PZ cathode is about 0.5 mg cm^{-2} and the volume of electrolyte used in each cell is 100 μL. The galvanostatic charging/discharging measurements were conducted on a LAND CT3001A battery testing system with a voltage window of 0.2–2.2 V (*vs.* Mg^{2+}/Mg). The galvanostatic intermittent titration technique (GITT) test was performed on the same battery testing system and the GITT curves were assessed under a constant current pulse of 100 mA g^{-1}, featuring pulse and relaxation intervals of 10 and 20 minutes, respectively. The cyclic voltammetry (CV) curves were collected on a Gamry Interface1010E electrochemical workstation. The electrochemical impedance spectroscopy (EIS) tests were conducted in a frequency range of 0.01–100000 Hz with applied amplitude of 0.005 V on the same electrochemical

workstation.

Computational details and methodology

The molecular geometries of PP14 cation, HDMS and TFSI anions, and THF solvent molecule in two electrolyte systems of $Mg(HMDS)_2$-$MgCl_2$/THF and $Mg(HMDS)_2$-$MgCl_2$/THF-0.5PP14TSFI were first optomized by the Gaussian 16 package at B3LYP/6-311+G(d) level of theory[S2]. The second-order Møller-Plesset perturbation[S3] method and the correlation-consistent polarized valence cc-pVTZ(-f) basis set[S4] were used to fit the molecular electrostatic potential at atomic centers to calcute the atomic partial charges on the above solvent molecules. Based on the previous work[S5], the atomistic AMBER force field were employed for all ions and molecules. The cross-interaction parameters between different atomic types were obtained based on the Lorentz-Berthelot combination rule.

Molecular dynamic (MD) simulations were performed using GROMACS software package with cubic periodic boundary conditions[S6]. Classic leapfrog integration Verlet algorithm[S7] with a time step of 1.0 fs was used to integrate the motion equations of all atoms. A cutoff radius of 1.6 nm was applied for short-range van der Waals interactions and real-space electrostatic interactions. Long-range electrostatic interactions in reciprocal space were handled by using the particle-mesh Ewald (PME) summation method[S8] with an interpolation order of 5 and a Fourier grid spacing of 0.15 nm. Steepest descent algorithm was first used to minimize the energy of all simulation systems, followed by the gradual temperature reduction from 700 K to room temperature (300 K) within 10 ns. Subsequently, the annealed simulation systems were equilibrated in an isothermal-isobaric

(NPT) ensemble for 10 ns, where Nosé-Hoover thermostat and a Parrinello-Rahman barostat with coupling constants of 0.4 and 0.2 ps were employed to control the temperature at 300 K and the pressure at 1 atm. Atomistic simulations were further performed in a canonical ensemble (NVT) for 30 ns, with simulation trajectories recorded at intervals of 100 fs for structural and dynamical analysis.

Table S1. Two electrolyte model systems with and without PP14TFSI simulated in this work.

	$Mg(HMDS)_2$-$MgCl_2$/THF	$Mg(HMDS)_2$-$MgCl_2$/THF-0.5PP14TSFI
No. of $MgCl_2$	90	65
No. of $Mg(HDMS)_2$	22	16
No. of THF	1116	806
No. of PP14TFSI	–	103
Total No. of atoms	15988	16497
System size	$(5.6881\ nm)^3$	$(5.7466\ nm)^3$

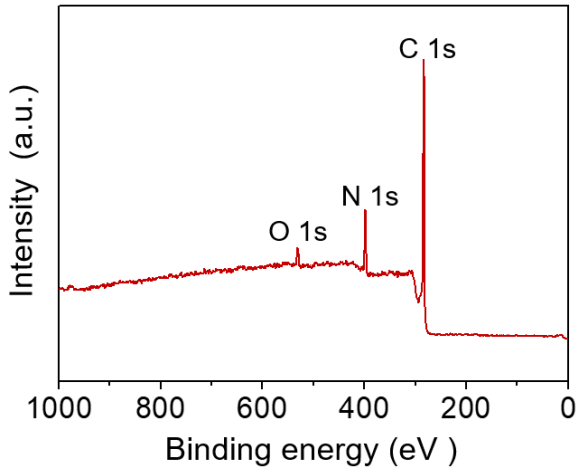

Fig. S1 XPS survey spectrum of phenazine.

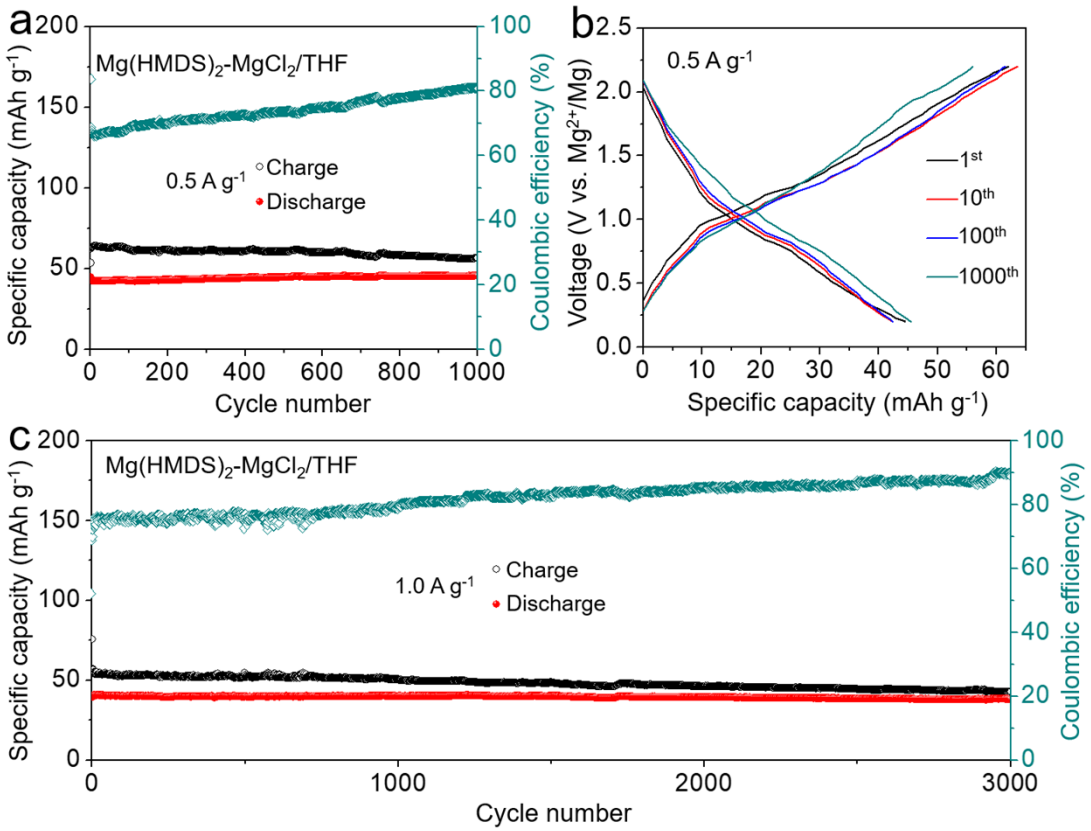

Fig. S2 Electrochemical performance of Mg/PZ cells with pristine GF separator and $Mg(HMDS)_2$-$MgCl_2$/THF electrolyte. (a, b) Cycling performance and the corresponding discharge-charge profiles at 0.5 A g^{-1}. (c) Long-term cycling stability at 1.0 A g^{-1}.

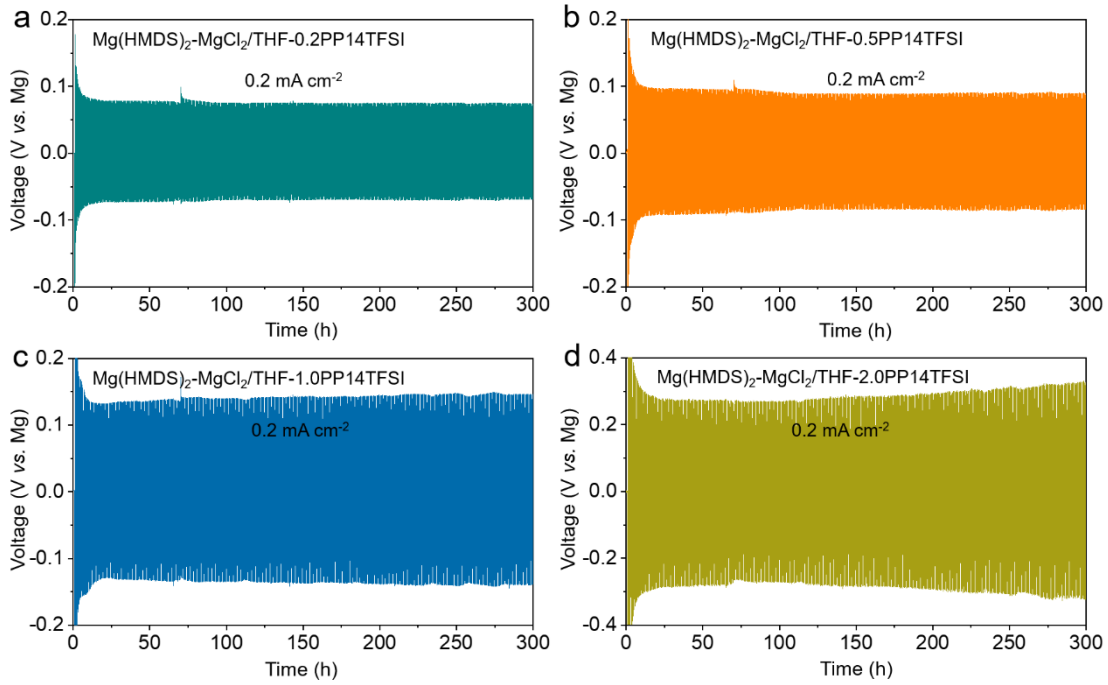

Fig. S3 Cycling performance of Mg||Mg cells at 0.2 mA cm^{-2} using different electrolytes of (a) $Mg(HMDS)_2$-$MgCl_2$/THF-0.2PP14TSFI, (b) $Mg(HMDS)_2$-$MgCl_2$/THF-0.5PP14TSFI, (c) $Mg(HMDS)_2$-$MgCl_2$/THF-1.0PP14TSFI, (d) $Mg(HMDS)_2$-$MgCl_2$/THF-2.0PP14TSFI, respectively.

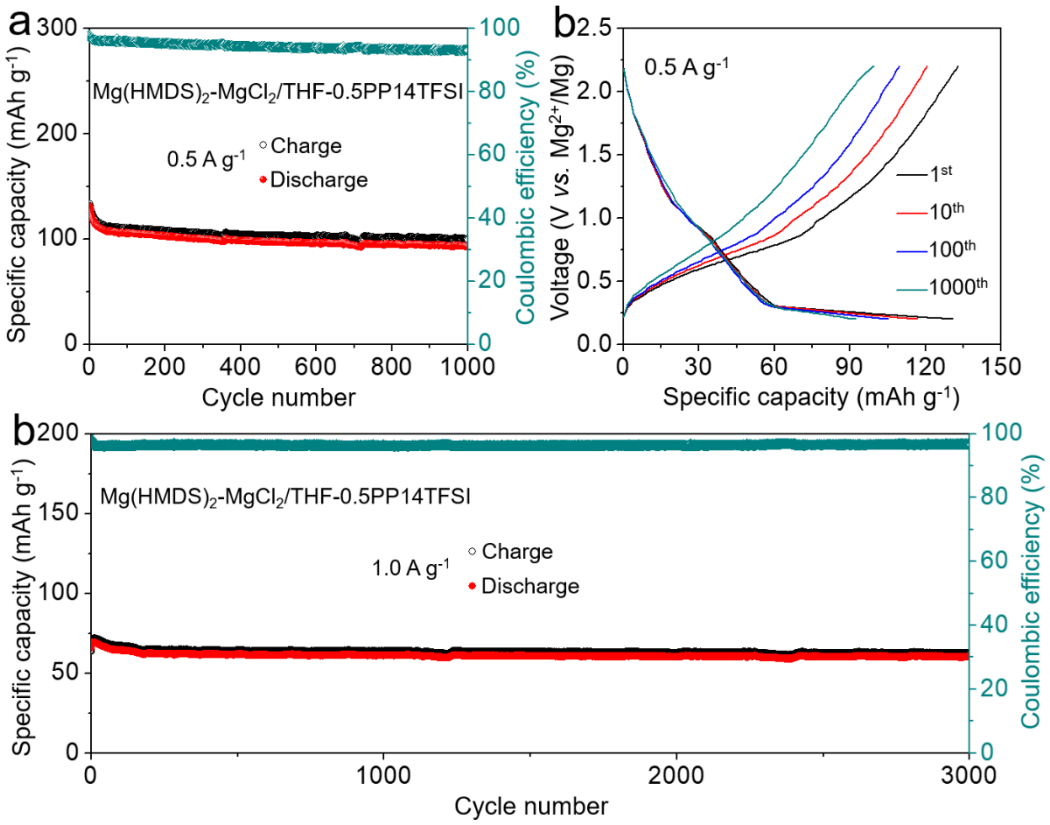

Fig. S4 Electrochemical performance of Mg/PZ cells with pristine GF separator and $Mg(HMDS)_2$-$MgCl_2$/THF-0.5PP14TSFI electrolyte. (a, b) Cycling performance and the corresponding discharge-charge profiles at 0.5 A g^{-1}. (c) Long-term cycling stability at 1.0 A g^{-1}.

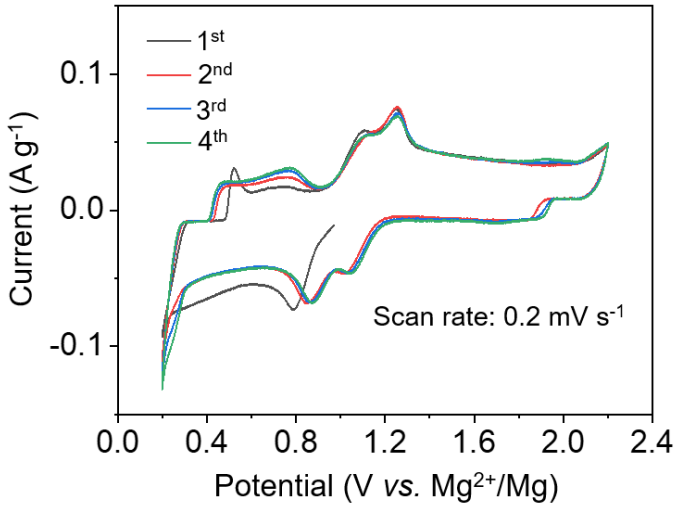

Fig. S5 CV curves of Mg/PZ cells with Graphene@PVP/GF separator and $Mg(HMDS)_2$-$MgCl_2$/THF-0.5PP14TSFI electrolyte at a scan rate of 0.2 mV s^{-1} between 0.2 and 2.2 V *vs*. Mg^{2+}/Mg.

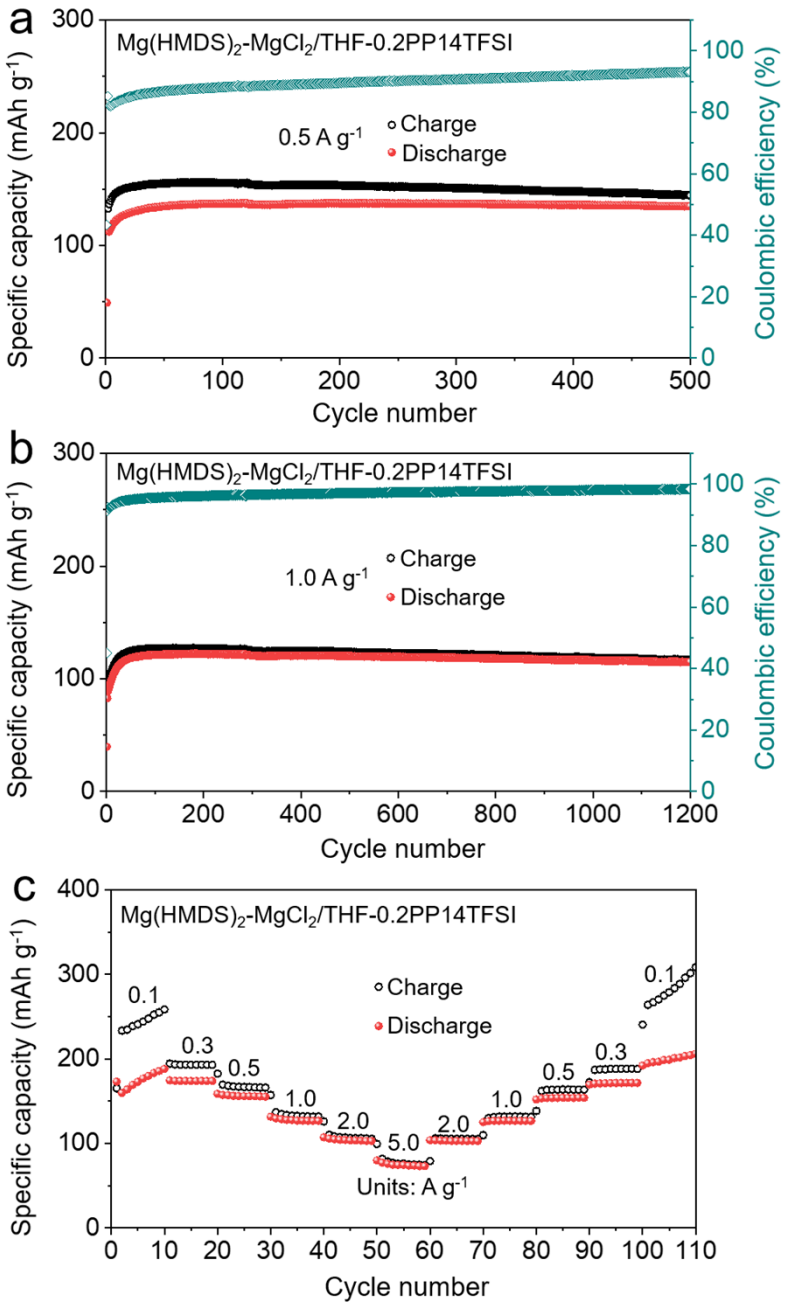

Fig. S6 Electrochemical performance of Mg/PZ cells using Graphene@PVP/GF separator and $Mg(HMDS)_2$-$MgCl_2$/THF-0.2PP14TSFI electrolyte. (a, b) Cycling performance at the current densities of 0.5 A g^{-1} and 1.0 A g^{-1}. (c) Rate capability at different current densities.

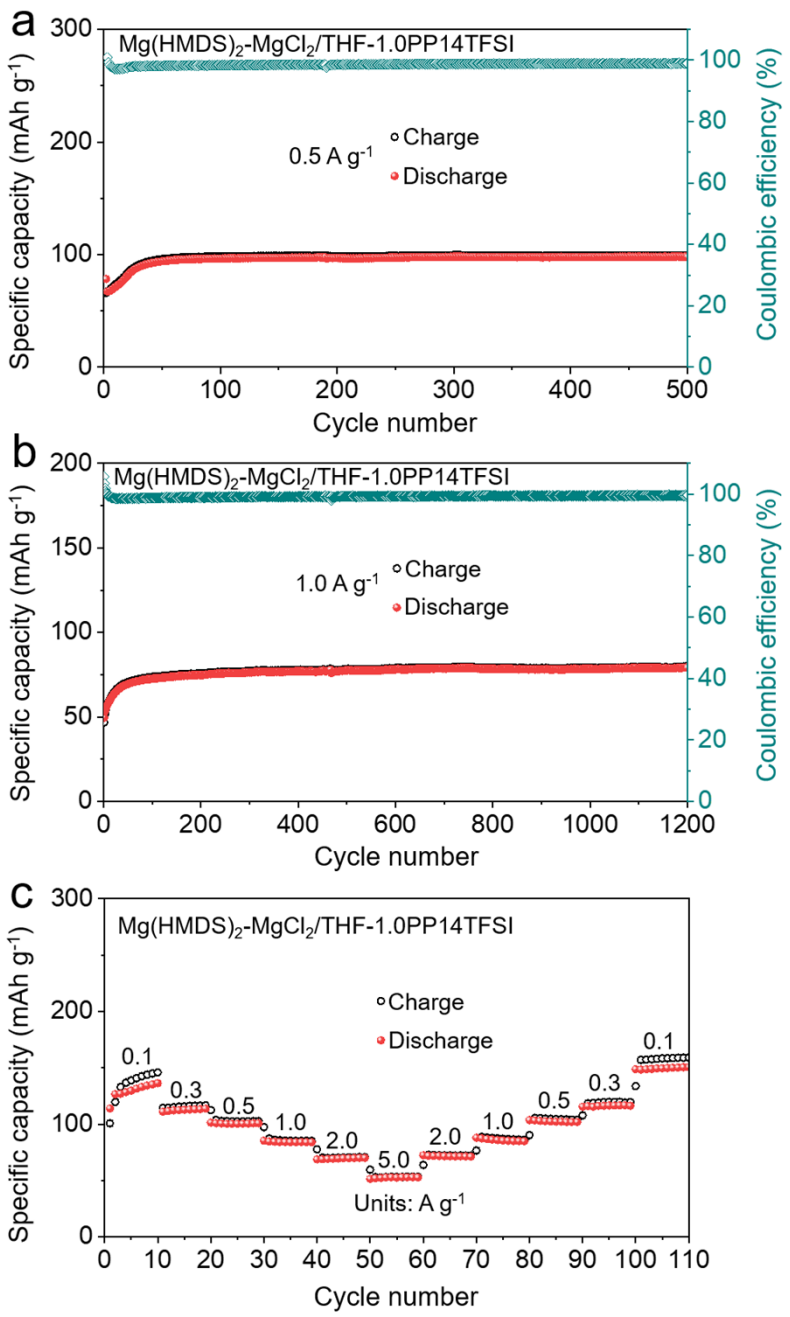

Fig. S7 Electrochemical performance of Mg/PZ cells using Graphene@PVP/GF separator and $Mg(HMDS)_2$-$MgCl_2$/THF-1.0PP14TSFI electrolyte. (a, b) Cycling performance at the current densities of 0.5 A g^{-1} and 1.0 A g^{-1}. (c) Rate capability at different current densities.

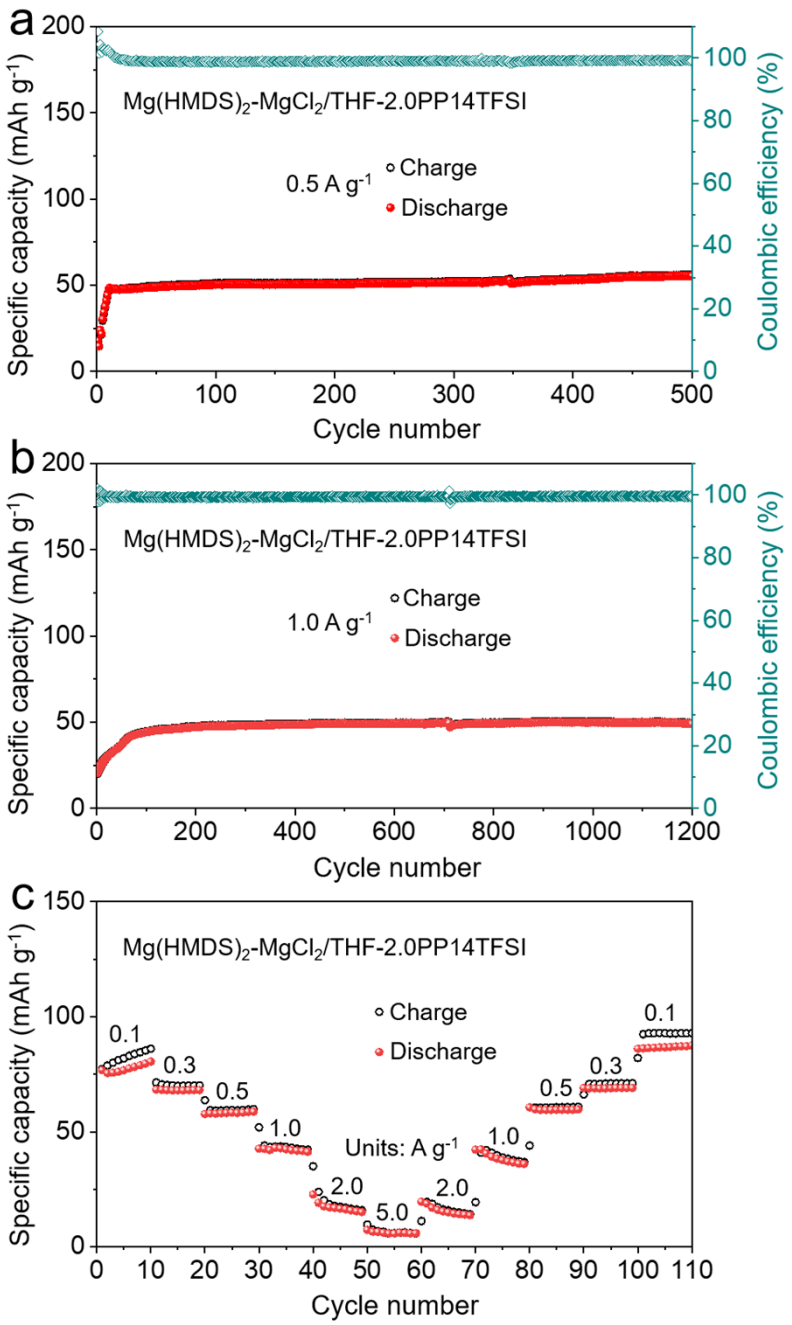

Fig. S8 Electrochemical performance of Mg/PZ cells using Graphene@PVP/GF separator and $Mg(HMDS)_2$-$MgCl_2$/THF-2.0PP14TSFI electrolyte. (a, b) Cycling performance at the current densities of 0.5 A g^{-1} and 1.0 A g^{-1}. (c) Rate capability at different current densities.

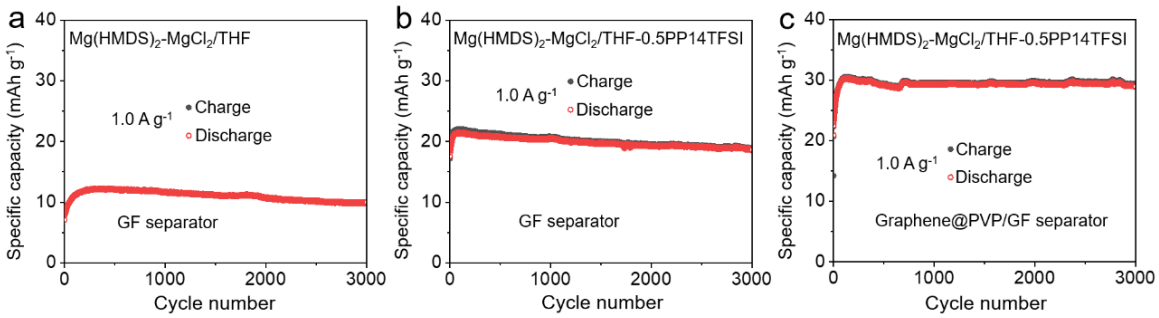

Fig. S9 Electrochemical performance of cathode without PZ at 1.0 A g^{-1} in three different cells: (a) one with a GF separator in $Mg(HMDS)_2$-$MgCl_2$/THF electrolyte, (b) another with a GF separator in $Mg(HMDS)_2$-$MgCl_2$/THF-0.5PP14TFSI electrolyte, and (c) the third with a Graphene@PVP/GF separator in $Mg(HMDS)_2$-$MgCl_2$/THF-0.5PP14TFSI electrolyte.

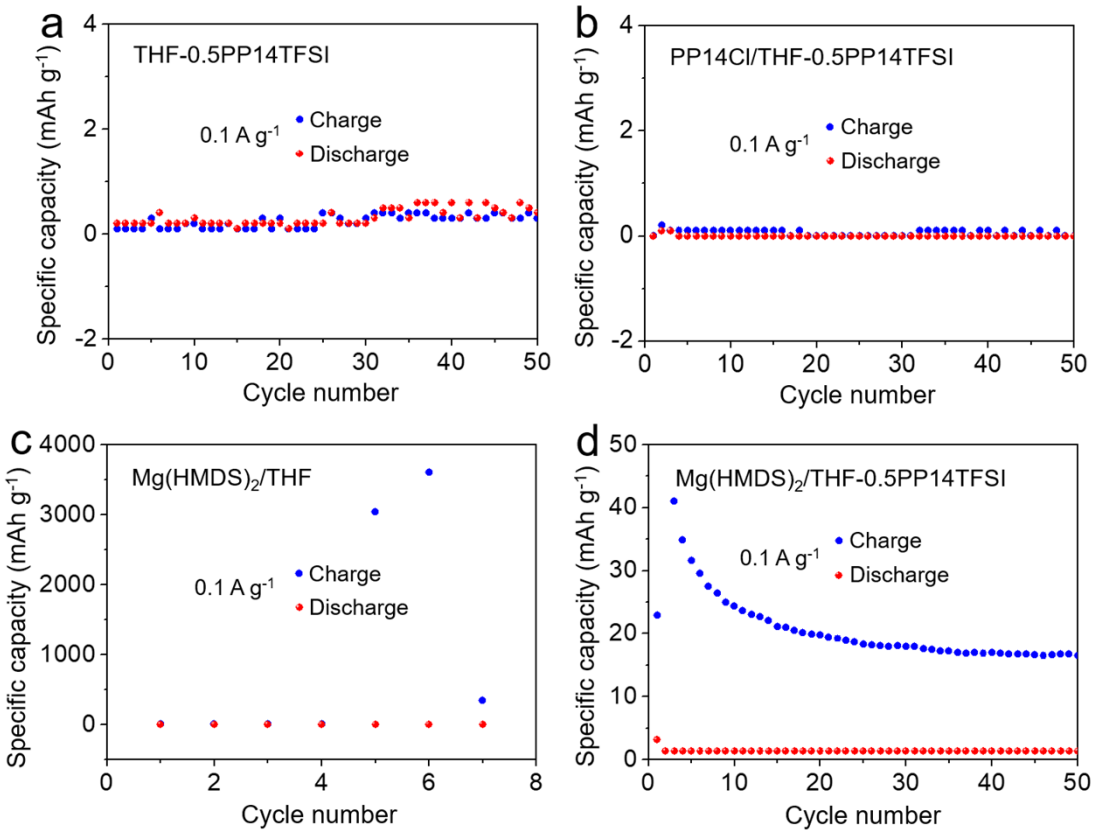

Fig. S10 Electrochemical performance of PZ electrode tested at 0.1 A g^{-1} in different electrolytes of THF-PP14TFSI, PP14Cl/THF-PP14TFSI, $Mg(HMDS)_2$/THF, and $Mg(HMDS)_2$/THF-PP14TFSI.

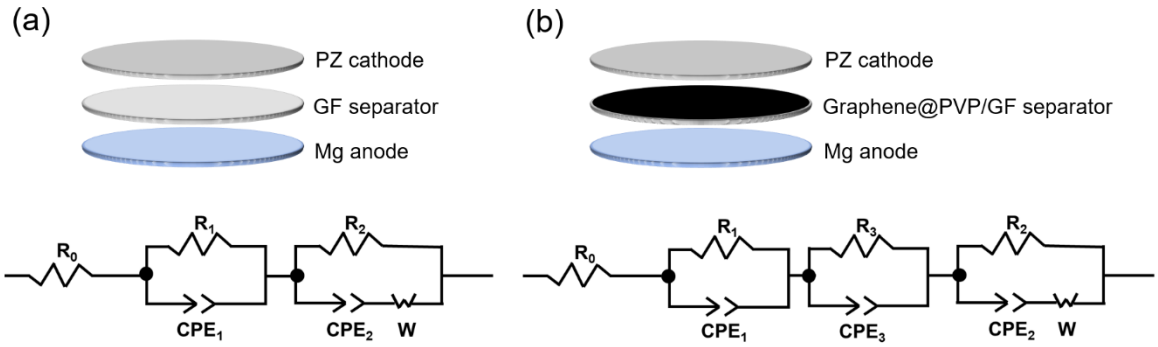

Fig. S11 Equivalent circuits of the Mg//PZ cells using (a) conventional, and (b) Graphene@PVP-modified GF separators, recorded at open circuit voltage, respectively.

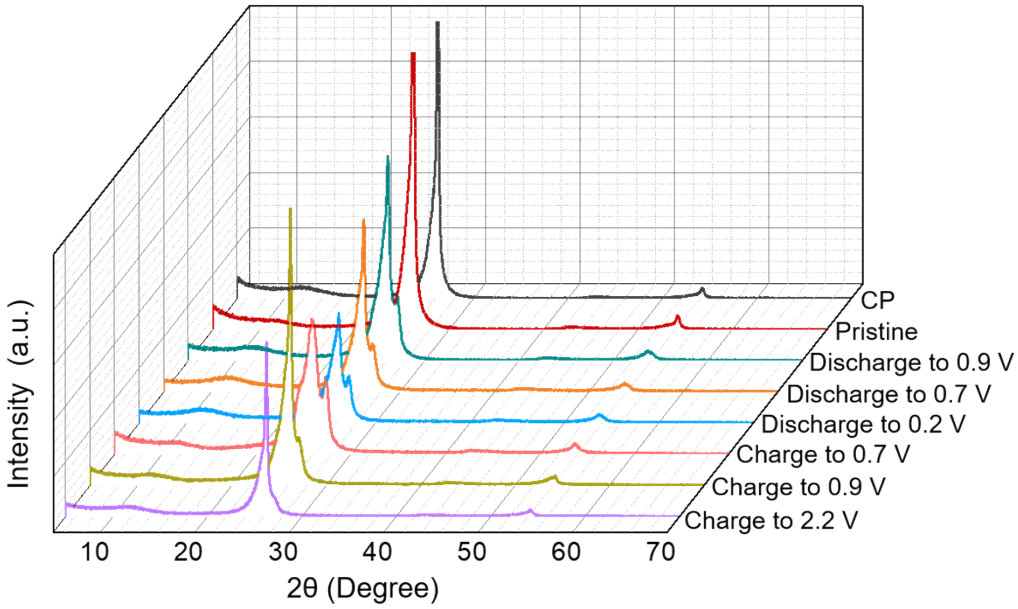

Fig. S12 Ex XRD patterns of PZ cathode under different discharging/charging states at a current density of 0.2 A g^{-1}.

References:

1. X. Xue, R. Chen, C. Yan, P. Zhao, Y. Hu, W. Kong, H. Lin, L. Wang and Z. Jin, *Adv. Energy Mater*., 2019, **9**, 1900145.
2. J. R. Frisch, G. W. Trucks, H. B. Schlegel, G. E. Scuseria, M. A. Robb, J. R. Cheeseman, G. Scalmani, V. Barone, G. A. Petersson, H. Nakatsuji, X. Li, M. Caricato, A. V. Marenich, J. Bloino, B. G. Janesko, R. Gomperts, B. Mennucci and D. J. Hratch Gaussian 16, Revision C.01 Gaussian, Inc., Wallingford CT 2016.
3. R. J. Iuliucci, J. D. Hartman and G. J. Beran, *J. Phys. Chem. A*, 2023, **127**, 2846-2858.
4. M.M. Kermani and D. G. Truhlar, *Chem. Phys. Lett.*, 2023, **825**, 140575.
5. F. U. Shah, S. Glavatskih, O. N. Antzutkin, A. Laaksonen, *J. Phys. Chem. B*, 2014, **118**, 8711-8723.
6. M. J. Abraham, T. Murtola, R. Schulz, S. Páll, J. C. Smith, B. Hess and E. Lindahl, *SoftwareX*, 2015, **1**, 19-25.
7. M. A. Cuendet and W. F. Gunsteren, *J Chem. Phys.*, 2007, **127**, 184102.
8. Y. Wang, Y. Zhu, Z. Lu, A. Laaksonen, *Soft Matter*, 2018, **14**, 4252-4267.